Calibration of a material behavior model for the simulation of multi-leaf stone masonry structures: Experimental case study application

B. Silva, A. Pappas, M.R. Valluzzi, F. da Porto, C. Modena
University of Padova, Italy

SUMMARY:
This paper presents the numerical simulation of shaking table tests performed on a house built with three-leaf stone masonry in scale 2:3. The masonry properties were simulated using a continuum damage behaviour model, [Faria et al., 1998], calibrated based on the results of shear-compression tests, [Mazzon, 2010]. The model properties and boundary conditions of the house were further verified with the dynamic identification tests performed on the house during the experimental campaign. The applied macro-modelling strategy using a non-linear continuum damage behaviour model was capable of realistically simulating the behaviour of the model house under dynamic loads and more particularly the accumulative development of the damage in the structure and the corresponding crack pattern, showing however limitations when trying to reproduce phenomena as the rocking behaviour of the house which induce high displacements.

Keywords: Shaking table, stone masonry, FEM, damage model

1. INTRODUCTION

The shaking table tests which are simulated numerically were performed on a house built in reduced scale (2:3) with three-leaf stone masonry according to a traditional technique and strengthened with hydraulic lime grout injection. The tests on the house were carried out under bi-directional seismic actions with increasing and sequential levels of Peak Ground Acceleration (PGA). The masonry properties were simulated using a continuum damage behaviour model [Faria et al., 1998], calibrated based on the results of shear-compression tests performed on masonry panels recovered from the building after the shaking table test, [Mazzon, 2010]. Numerical modal analyses were also carried out as part of the calibration procedure, based on the results of the experimental dynamic identification tests. The numerical results, namely the seismic resistance, the displacement capacity and the damage state (crack pattern) of the masonry house for the different excitation levels, are analysed and compared to the experimental results, allowing to assess the capacity of this type of modelling methodology and behaviour models to simulate the global behaviour of such construction.

2. DESCRIPTION OF THE SHAKING TABLE TEST

2.1. Description of the tested house

The experimental campaign consisted in a series of shaking table tests on a scale 2:3 stone masonry house (SH) strengthened with natural hydraulic lime grout injection, Figure 2.1, [Mazzon, 2010]. The model presents a rectangular floor plan (2.40x2.80m) and two floors with an overall height of 3.60m (1.80m per floor). The façades were constructed with different openings in order to achieve an asymmetric behaviour with high torsional effects.

Prospect A Prospect B Prospect C Prospect D

Figure 2.1. Different prospects of the house.

The floors were composed of timber beams creating a non-rigid diaphragm. Steel ties were also used at both floor levels in order to avoid the out-of-plane behaviour of the walls. In total, six tie beams were used in each floor: three fixed to timber beam heads anchored to the walls and three placed in the orthogonal direction in respect to those. Timber lintels were used over the openings of the structure. The structure consists of three-leaf stone masonry walls with a total thickness of 33.0cm. The external leaves had a thickness of 12.0cm and they were built with rough limestone and natural hydraulic lime mortar, while the inner core was built with limestone fragments and strengthened with hydraulic lime based grout.

The whole masonry structure was built on a RC basement, 40.0cm height by the thickness of the walls, which was used for transporting the structures and fixing them on the shaking table. In order to simulate the effect of the live load in the scaled specimen and respect the similitude relationship, additional masses of 500 kg had to be added to both floors, [Tomaževič and Velechovsky, 1992].

2.2. Loading conditions

The base seismic signal that was used on the experimental analysis is part of the Montenegro earthquake of 15/4/1979. A dynamic test on a scale 2:3 model imposes that the acceleration and the time of the signal had to be multiplied and divided by 3/2, respectively, Figure 2.2. The experimental tests on the house were carried out with increasing levels of Peak Ground Acceleration (PGA), (0.05g step) until a maximum PGA of 0.70g, by simply scaling the initial input accelerations to the desired step level. Until a PGA level of 0.55g the load was applied in both directions while from 0.55g to 0.70g the load was applied only in the X direction.

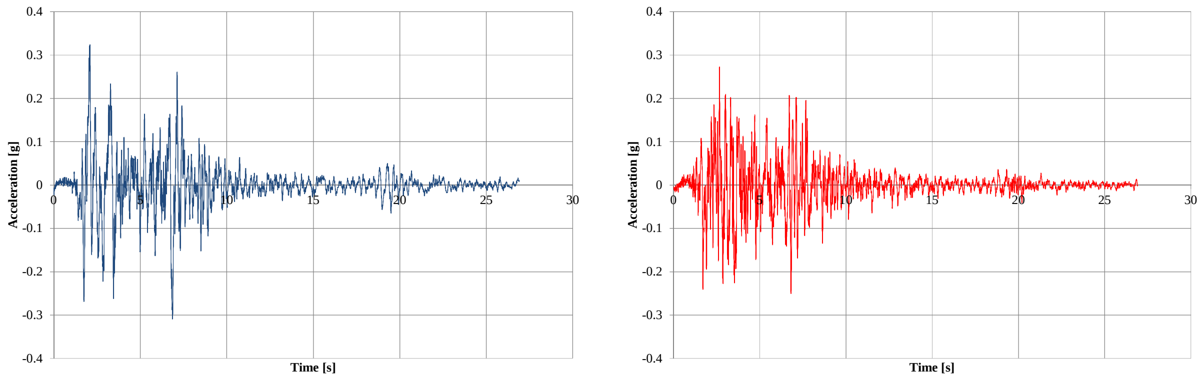

(a) (b)

Figure 2.2. Elaborated seismic inputs for the 2:3 scale models based on 1979 Montenegro earthquake on the (a) X and (b) Y directions.

3. NUMERICAL MODELLING

3.1. Numerical model description

The numerical model, Figure 3.4a, was created in the finite elements program Cast3M [CEA, 1990]. The masonry was simulated using 8 nodes volumetric elements (CUB8) and the non linear continuum damage model [Faria et al., 1998]. The timber elements over the openings were also simulated using 8 nodes volumetric elements (CUB8) but with linear elastic properties. The timber floors were simulated using 4 node shell elements (COQ4) and also considering linear elastic properties. The additional mass (500kg) of the steel plates on each floor was taken into account on the specific weight of the floors (3100kg/m^3).

The steel ties were simulated using 2 node bar elements (BARR) with a unidirectional linear elastic behaviour (null compression resistance) with the objective of realistically reproducing the elements behaviour. The steel ties mechanical characteristics were defined according to the EN 1993-1-1:1998 [CEN, 1998], and the bars unidirectional characteristics were defined by the material model FRAGILE_UNI, [Combescure, 2000], implemented in Cast3M. The timber beams were also simulated with 2 node bar elements; the ones anchored to the walls were simulated considering a linear elastic behaviour, while for the other beams a unidirectional behaviour (working only under compression) was adopted. The reinforced concrete beam was simulated considering linear elastic and isotropic properties taken from EN 1992-1-1:2004, [CEN, 2004]. The properties of all the implemented finite element types are presented in Table 3.1.

Preliminary analysis showed that the interface between the masonry leaves had to be simulated; considering a homogeneous material throughout the whole thickness of the walls lead to very small displacements. The interfaces were simulated through a linear joint element defined by the transversal (k_t = 1.17·108Pa/m) and normal (k_n = 1·1011Pa/m) stiffness based on the experimental work of Costa [2009]. Analyses considering a Mohr-Coulomb friction non-linear joint element were also performed, but since no significant differences were found in the behaviour of the houses when compared to model with the linear joint model, only the second model was used.

Table 3.1. Properties of the structural elements of the houses.

	Elements	**ρ [kg/m^3]**	**S [m^2]**	**f_t [N/mm^2]**	**f_c [N/mm^2]**	**e [m]**	**E [GPa]**	**ν [-]**
RC beam	CUB8	2900	-	-	-	-	29.0	0.20
Timber lintels	CUB8	415	-	-	-	-	10.5	0.37
Timber floors	COQ4	3100	-	-	-	0.05	10.5	0.37
Timber beams - Anchored	SEG2	415	0.108	-	-	-	10.5	0.37
Timber beams - Not Anchored	SEG2	415	0.108	0.0	20.0	-	10.5	0.37
Steel	SEG2	7850	7.9x10^{-5}	500.0	0.0	-	210.0	0.30

3.1.1. Masonry properties calibration

The parameters of the continuum damage behaviour model adopted in the simulation of the masonry of the SH were calibrated based on the results of the shear-compression tests performed on three masonry panel's extracted from the tested building, as described in Mazzon [2010]. The specimens, obtained from the building model, had a mean overall thickness of 33.0cm and slenderness ratios of 0.9, 1.4 and 1.5. The geometrical characteristics and the applied pre-compression loads of each panel are presented in Table 3.2.

Table 3.2. Shear-compression test matrix, [Mazzon, 2010].

Specimens	***Vertical Stress σ'₀ [N/mm²]***	***Slenderness (h/l)***	***Thickness [mm]***	***Width [mm]***	***Height [mm]***
S2	2.0	0.9	325	1453	1370
S4	1.0	1.4	331	923	1275
S5	2.0	1.5	328	929	1381

A representative material behaviour law (in tension and compression), capable of reproducing the in-plane behaviour under the different applied pre-compression levels, was defined for the tested masonry specimens, Figure 3.1. The corresponding model parameters are presented in Table 3.3.

Table 3.3. Parameter values that resulted from the calibration process based on the shear-compression tests.

Parameters		***2:3R [Mazzon, 2010]***
YOUN	Elastic modulus [N/m^2]	$3.7 \cdot 10^9$
NU	Poisson ratio [-]	0.12
RHO	Density [kg/m^3]	2500
GVAL	Tensile fracture energy [J]	50
FTUL	Tensile stress [N/m^2]	$0.15 \cdot 10^6$
REDC	Drop factor for peak tensile stress [-]	0
FC01	Elastic limit compressive stress [N/m^2]	$-2.2 \cdot 10^6$
RT45	Equi-biaxial compressive Ratio [-]	1
FCU1	Compressive peak stress [N/m^2]	$-5.0 \cdot 10^6$
EXTU	Ultimate limit strain [-]	-0.02
EXTP	Reference strain for plastic parameter [-]	-0.0045
STRP	Reference stress for plastic parameter [-]	$-2.2 \cdot 10^6$
EXT1	Fitting point 1 - Strain [-]	-0.0045
STR1	Fitting point 1 - Stress [N/m^2]	$-4.0 \cdot 10^6$
EXT2	Fitting point 2 - Strain [-]	-0.023
STR2	Fitting point 2 - Stress [N/m^2]	$-4.9 \cdot 10^6$
NCRI	Tensile softening criteria [-]	1

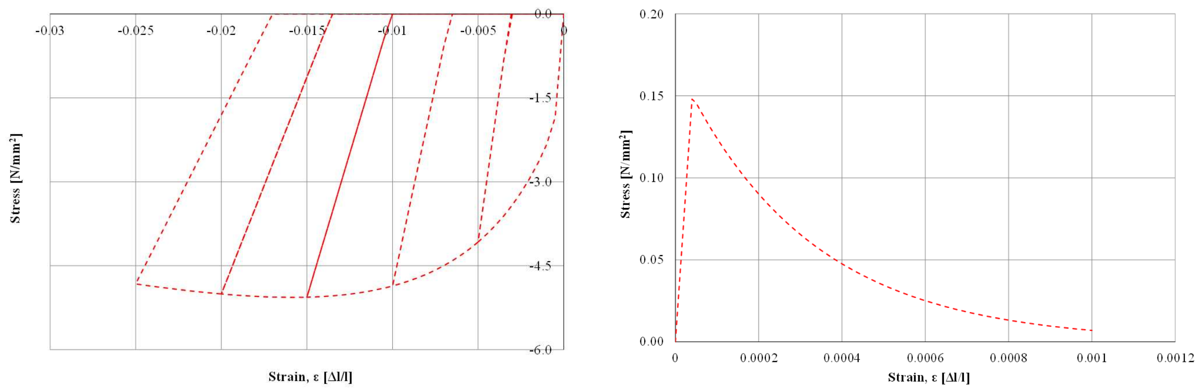

Compressive behaviour | Tensile behaviour

Figure 3.1. Material behaviour laws for the SH masonry.

As can it be seen from the response curves comparison in Figure 3.2, which represents the in-plane force versus horizontal displacement of the panels under different pre-compression loads, and the results summarized in Table 3.4, a good fit was achieved between the numerical and the experimental results. The calibrated model was able to simulate the initially elastic stiffness (k), the maximum horizontal loads (H_{max}) and also the displacement capacity. Both the resistance ratio ($H_{max,n}/H_{max,e}$) and the displacement capacity ratios ($\delta_{Hmax,n}/\delta_{Hmax,e}$ and $\delta_{u,n}/\delta_{u,e}$) are approximately 1 for all tested panels. Only the dissipated energy is not well simulated by the model.

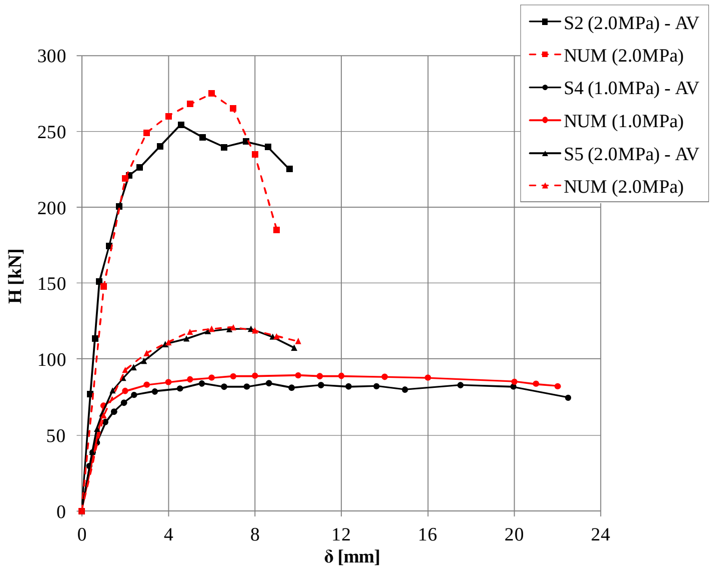

Figure 3.2. Experimental and numerical response curves (force vs. displacements) of the shear-compression tests - envelope of the hysteretic curves.

Table 3.4. Comparison of the numerical and experimental maximum horizontal load (H_{max}), displacement for maximum load (δ_{Hmax}) and displacement at ultimate state (δ_u), for the SH masonry.

Specimens	Experimental			Numerical			$H_{max,n}$ / $H_{max,e}$ [-]	$\delta_{Hmax,n}$ / $\delta_{Hmax,e}$ [-]	$\delta_{u,n}$ / $\delta_{u,e}$ [-]
	$H_{max,e}$ [kN]	$\delta_{Hmax,e}$ [mm]	$\delta_{u,e}$ [mm]	$H_{max,n}$ [kN]	$\delta_{Hmax,n}$ [mm]	$\delta_{u,n}$ [mm]			
S2 (2.0MPa)	256	5.1	9.6	275	6.0	9.0	1.1	1.2	0.94
S4 (1.0MPa)	88	11.3	22.0	89	12.0	22.0	1.0	1.1	1.0
S5 (2.0MPa)	122	7.1	9.8	121	7.0	10.0	0.99	0.99	1.0
Average							**1.0**	**1.1**	**0.98**

3.2 Modal analysis

3.2.1. Calibration of the masonry properties

A modal identification of the strengthened house was performed. This identification based on the ambient vibration tests performed on the house allowed the verification of the elastic masonry properties for the following boundary conditions: (A) placed outside the shaking table and simply supported on the floor; (B) after being placed on the table when this is on the locked position. Afterwards, springs simulating the table effect were also calibrated based on the ambient vibration tests performed on the house placed on the shaking table, but on the unlocked position (C). The model properties and boundary conditions were calibrated by fitting the numerical frequencies and mode shapes to the first three experimental global vibration modes shapes.

The model parameters resulting from this calibration are presented in Table 3.5 and the modal shapes in Figure 3.3. In order to take into account the effect of the shaking table in the model response, in particular the possibility of the table to rotate along the in-plane orthogonal axis, it were considered as boundary conditions vertical springs at the base ($k_{zx} = 4.5 \cdot 10^7 N/mm^2$, $k_{zy} = 11.5 \cdot 10^7 N/mm^2$, and $k_{zg} = 11.5 \cdot 10^7 N/mm^2$), as schematized in Figure 3.4.

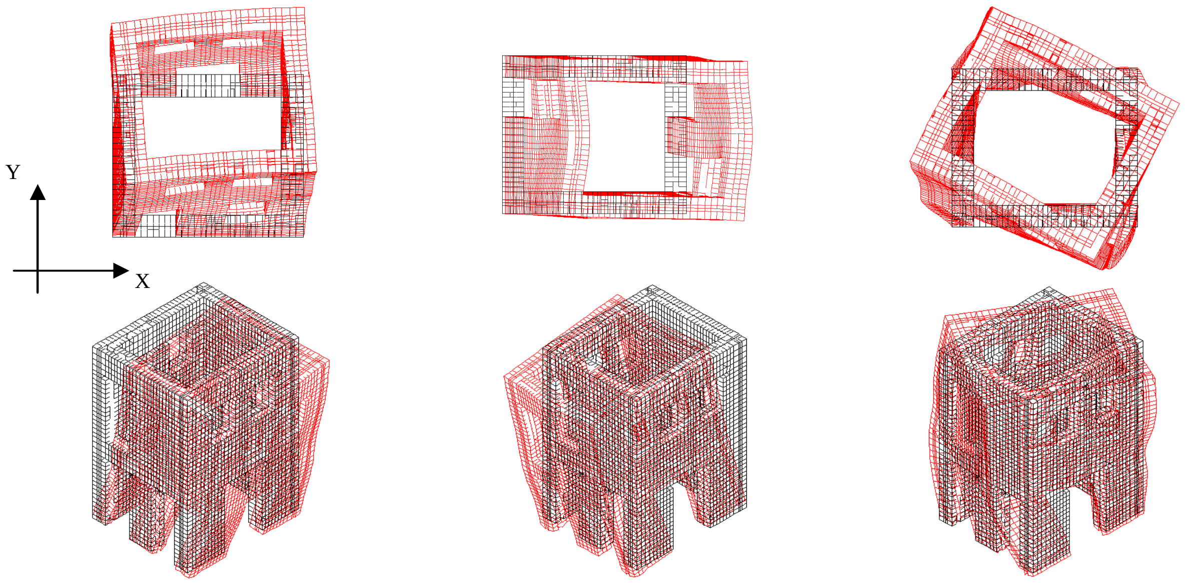

1st flexural mode - Y direction   2nd flexural mode - X direction   Torsional mode.

Figure 3.3. Numerical global mode shapes of the houses.

Table 3.5. Parameter values that resulted from the calibration process based on dynamic identification tests under (B) conditions - SH.

	Parameters	***SH (B)***
YOUN	Elastic modulus [N/m^2]	$1.7 \cdot 10^9$
NU	Poisson ratio [-]	0.12
RHO	Density [kg/m^3]	2500
GVAL	Tensile fracture energy [J]	50
FTUL	Tensile stress [N/m^2]	$0.15 \cdot 10^6$
REDC	Drop factor for peak tensile stress [-]	0
FC01	Elastic limit compressive stress [N/m^2]	$-3.0 \cdot 10^6$
RT45	Equi-biaxial Compressive Ratio [-]	1
FCU1	Compressive peak stress [N/m^2]	$-5.0 \cdot 10^6$
EXTU	Ultimate limit strain [-]	-0.02
EXTP	Reference strain for plastic parameter [-]	-0.01
STRP	Reference stress for plastic parameter [-]	$-4.95 \cdot 10^6$
EXT1	Fitting point 1 - Strain [-]	-0.01
STR1	Fitting point 1 - Stress [N/m^2]	$-4.95 \cdot 10^6$
EXT2	Fitting point 2 - Strain [-]	-0.019
STR2	Fitting point 2 - Stress [N/m^2]	$-5.05 \cdot 10^6$
NCRI	Tensile softening criteria [-]	1

Table 3.6. Comparison of the numerical and experimental frequencies - SH.

	EXPERIMENTAL Frequency [Hz]			**NUMERICAL Frequency [Hz]**		
Mode	**(A)**	**(B)**	**(C)**	**(A)**	**(B)**	**(C)**
1st - Flexural Y-Axis	12.1	8.8	7.3	11.6	8.9	7.3
2nd - Flexural X-Axis	15.5	11.5	8.6	15.2	11.7	8.6
3rd - Torsional	25.8	19.3	15.6	20.7	15.8	15.2

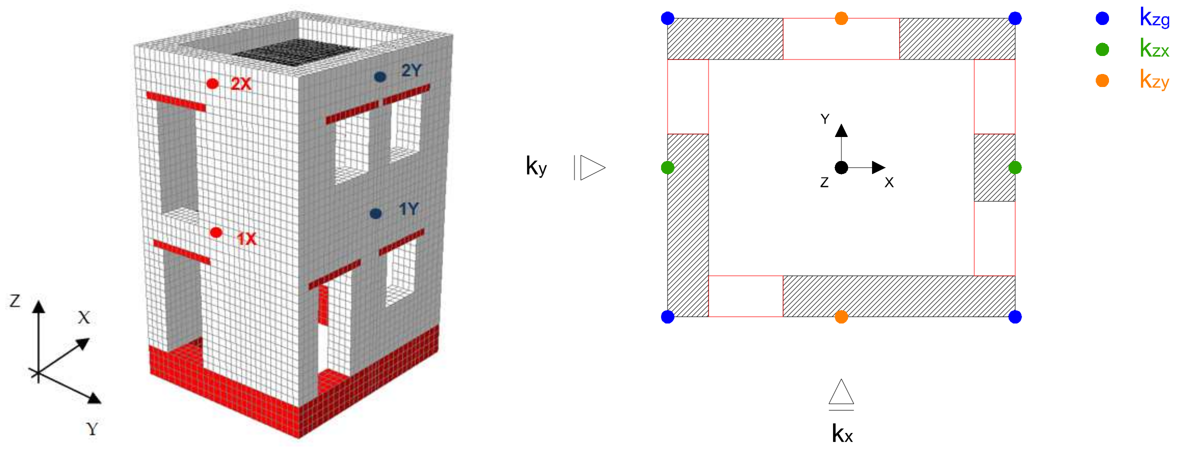

Figure 3.4. Numerical model of the house and control points (left). Boundary conditions (right).

3.3. Time history analysis

The bi-directional seismic actions considered in this study were the ones measured on the shaking table during the tests at the base of the house. These results are compared to the experimental ones, namely in terms of displacement profiles and damage propagation and patterns. The displacements were measured at the control points positioned on the floor levels, as illustrated in Figure 3.4.

3.3.1. Displacement profiles

In both experimental and numerical models and for all applied PGA levels, the first floor presented always higher drift, Figure 3.5, and more damage. Thus, the presented displacement profiles were drawn for, the step that corresponds to the highest storey drift obtained at the first floor level.
As the displacement profiles show, the numerically obtained displacements are smaller, i.e, the numerical model appears to be less deformable than the physical one, particularly in the X direction. This can be related to the rocking mechanism that influenced the overall behaviour of the house. This type of behaviour allows higher displacements with lower damage levels, which in fact was observed when comparing the experimental and numerical damage maps in the following section. For the different applied PGA levels the numerical model shows the same level of damage as in the experimental case but for lower displacement levels. In the graphs of Figure 3.5 the variation of the maximum drift (ψ) on the different control points for the applied PGA levels is presented.

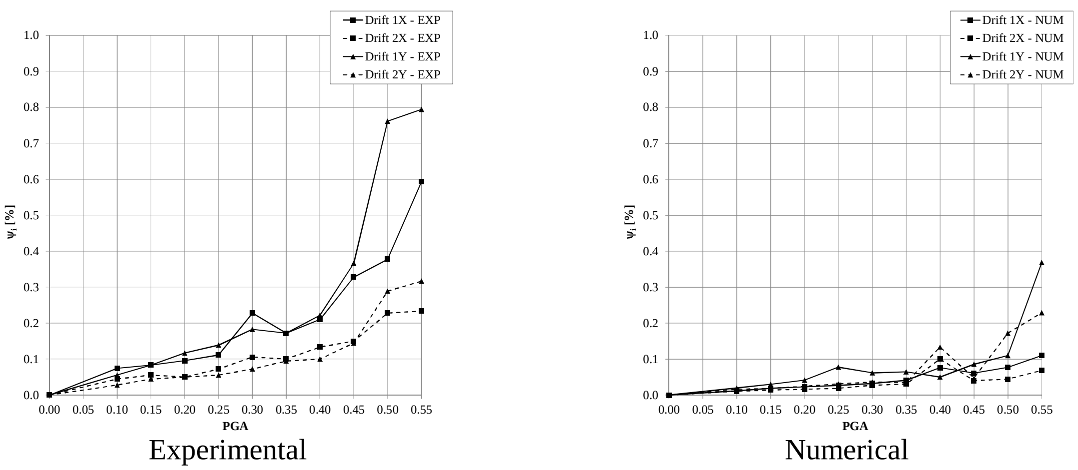

Figure 3.5. Drift (experimental and numerical) in the two main directions for the different applied PGA levels.

These graphs clearly show that in both the numerical and the experimental models the structure presents a high increase in deformation, particularly in Y direction (the smaller side), for a PGA level around 0.55g. This is related to the mechanism that formed in the pier at the first floor observed during the experimental tests (colour blue in Figure 3.6), and well captured by the numerical model (colour blue in Figure 3.7). Furthermore, the formation of this mechanism induces extensive damage at the first floor level as shown in the corner marked with a circle in Figure 3.**7** and Figure 3.8d and also observed experimentally, (colour red in Figure 3.6).

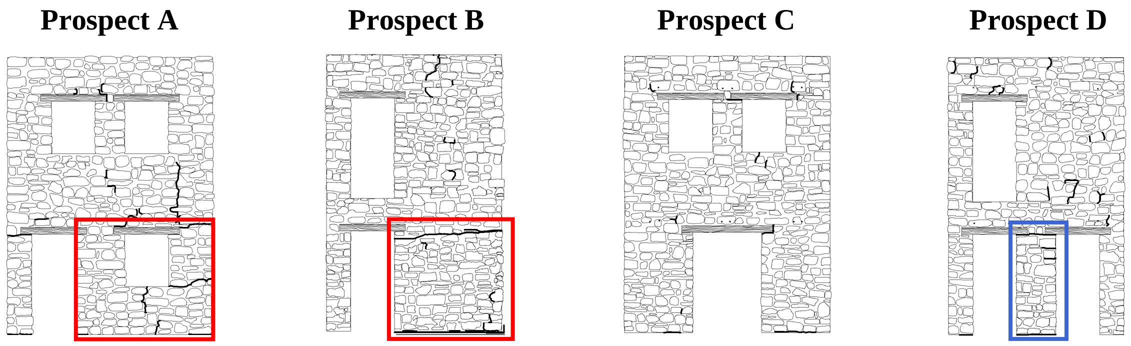

Figure 3.6. Damage pattern of SH at PGA 0.55g, [Mazzon, 2010].

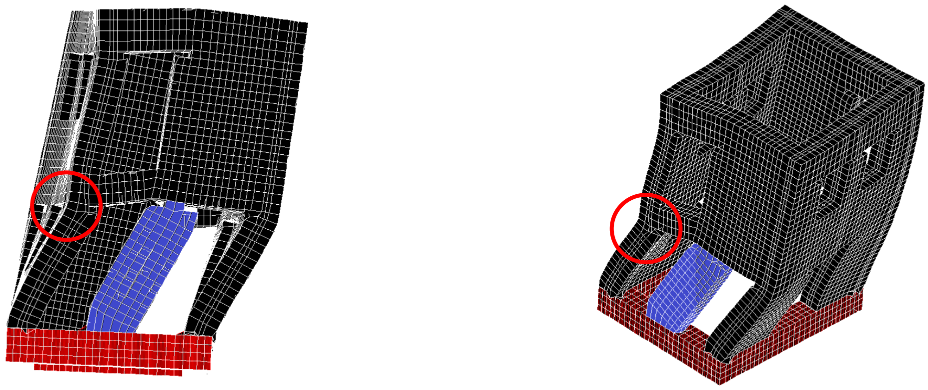

Figure 3.7. Numerical deformed shape for a PGA of 0.55g and corresponding to the highest drift at the first floor.

3.3.2. Damage propagation and crack pattern - Numerical vs Experimental

The tensile damage propagation and crack patterns obtained with the numerical model were compared to the ones observed during the experimental tests, for the different PGA levels, in order to assess if this macro-modelling strategy using this type of non-linear behaviour model is capable of realistically simulating the behaviour of the house under dynamic loads, in particular the accumulative development of the damage in the structure.

As it can be seen in Figure 3.8, the tensile damage propagation and patterns for the different PGA levels are very similar to those observed experimentally. However, there is higher damage due to the limitations in fully simulating damage. In comparison with the experimental results the model was able to capture very realistically the damage distribution and progression on the house during the tests. This is more evident principally in (i) the minor cracking for a PGA level of 0.25g, (ii) the collapse mechanism that started forming in the pier in Prospect D for a PGA level of 0.30g, which was aggravated during the following PGA levels and caused the end of the bi-directional load application on the real structure at 0.55g, (iii) the higher damage at the first floor of the model as result of the previously described sliding of the pier and finally (iv) the damage in the corners of the openings.

The numerical model was also able to simulate until a certain extent the rocking mechanism that affected the overall behaviour of the house, which is clear from the horizontal tensile damage formed at the base of the house, on the interface between the masonry and the RC beam, Figure 3.8. Furthermore, it is worth noticing that the model considers the material as homogeneous and, as so, does not take into account local phenomena such as the detachment of stone elements.

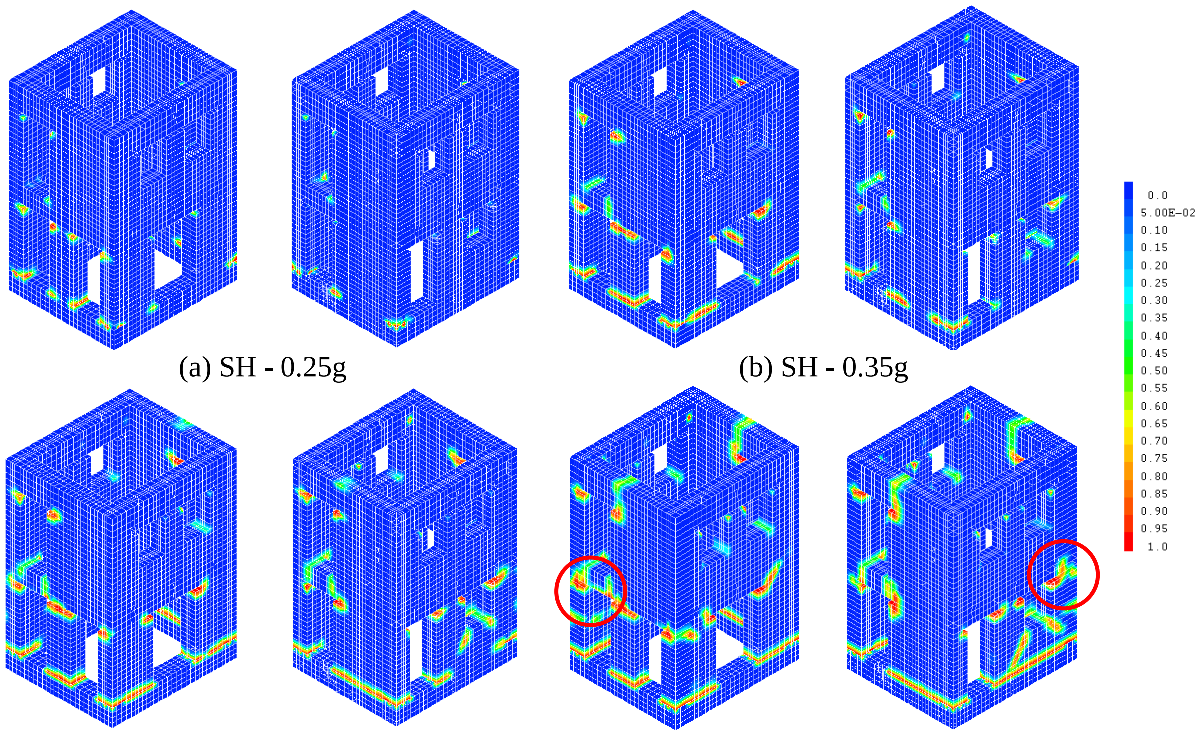

(a) SH - 0.25g (b) SH - 0.35g

(c) SH - 0.45g (d) SH - 0.55g

Figure 3.8. Tensile damage (d^+) maps for 0.25g, 0.35g, 0.45g and 0.55g.

4. CONCLUSIONS

The numerical simulation of shaking table tests performed on a three-leaf stone masonry house built in scale 2:3 and strengthened with hydraulic lime mortar was performed. The masonry properties were simulated using the continuum damage material behaviour model calibrated based on the results of shear-compression tests performed on masonry panels recovered from the building after the shaking table tests. The calibrated model allowed a good fit to the experimental results in terms of initial stiffness, maximum resistance and displacement capacity, although with lower energy dissipation. The masonry elastic properties in the numerical model were further calibrated with the dynamic identification tests performed during the experimental campaign. It took into consideration the effect of induced damage on the house during its transportation to the table by assuming elastic properties equivalent to a level of material solicitation. The effect of the shaking table on the behaviour of the house was also considered by introducing vertical springs at the base of the house.
The applied modelling strategy was able to reproduce the experimentally observed sequence of damage and crack patterns. In terms of displacement capacity, the house model was not as deformable as the real one. The numerical model was not able to reproduce the deformability shown by the real model in both directions mainly due to rocking mechanism that affected the global behaviour of the house.

ACKNOWLEDGEMENT

The authors would like to thank FCT (Fundação para a Ciência e a Tecnologia - The Foundation for Science and Technology) of Portugal and the NIKER project (New integrated knowledge based approaches to the protection of cultural heritage from Earthquake-induced risk) for the financial support provided for this research.

REFERENCES

CEA (1990). *Visual Cast3M - Guide d' utilisation*. France.
CEN (2004). EN 1992-1-1:2004. Eurocode 2: Design of concrete structures: General rules and rules for buildings.
CEN (1998). EN 1993-1-1:1998. Eurocode 3: Design of steel structures: General rules and rules for buildings.
Combescure, D. (2000). Rapport DM2S - Modélisation des structures de genie civil sous chargement sismique a l' aide de Castem 2000. France.

Costa C. (2004). *Implementation of the damage model in tension and compression with plasticity in Cast3m*. Laboratório ELSA, JRC, Italy.

Faria R. (1994). *Avaliação do comportamento sísmico de barragens de betão através de um modelo de dano contínuo*. PhD Thesis, Faculty of Engineering, University of Porto, Portugal.

Faria R., Oliver J., Cervera M. (1998). A strain-based viscous-plastic-damage model for massive concrete structures. *International journal of solids and structures.* **35**:**14**,1533-1558.

Mazzon, N. (2010). *Influence of Grout Injection on the Dynamic Behaviour of Stone Masonry Buildings*. PhD Thesis, University of Padova, Italy.

Silva B. (2012). *Diagnosis and strengthening of historical masonry structures: numerical and experimental analyses*. PhD Thesis, University of Padova, Italy.

Tomaževič, M. and Velechovsky, T. (1992). Some aspects of testing small-scale masonry building models on simple earthquake simulators. *Earthquake Engineering & Structural Dynamics*. **21:11**,945-963.